THE ASTROPHYSICAL JOURNAL, 443:238–244, 1995 April 10

SYNCHROTRON EMISSION FROM THE H_2O MASER SOURCE IN W3(OH)

M. J. REID, A. L. ARGON, C. R. MASSON, K. M. MENTEN, AND J. M. MORAN
Harvard-Smithsonian Center for Astrophysics, 60 Garden Street, Cambridge, MA 02138
Received 1994 July 26; accepted 1994 October 20

ABSTRACT

We present a study of the radio continuum source found near the position of the H_2O masers and the Turner-Welch source in the W3(OH) region. The source spectrum from 1.6 to 15 GHz exhibits a power law with spectral index -0.6. The continuum source is elongated in the east–west direction and its size decreases linearly with increasing frequency. These observations provide strong evidence for synchrotron emission from an inhomogeneous source.

The elongated continuum source is coincident within 0.″1 of the center of expansion of the H_2O masers and is aligned with the dominant H_2O outflow pattern. A possible model for the system includes an early-type star with a fast collimated wind that drives a jetlike outflow. Fast shocks in the wind or jet accelerate electrons, via a first-order Fermi process, to relativistic speeds necessary for synchrotron emission. The jet impinges on the surrounding molecular material and shocks and accelerates this material, leading to the motions observed in the H_2O masers.

Subject headings: ISM: individual (W3) — ISM: jets and outflows — masers — radiation mechanisms: nonthermal — radio continuum: ISM

1. INTRODUCTION

Interstellar H_2O masers are well-established signposts for the formation of both low-mass and high-mass stars. In low-mass star-forming regions, H_2O masers are associated with T Tauri, or other pre–main-sequence, stars. However, for high-mass star-forming regions the nature of the star(s) responsible for exciting the masers is largely unknown. Since these H_2O masers can have isotropic luminosities approaching 1 $L_\odot$ in the 22 GHz transition alone, a very luminous exciting source is required. Proper motions of the maser spots usually show them to be expanding, predominantly radially, from a single position (Genzel et al. 1981; Reid et al. 1988; Gwinn, Moran, & Reid 1992) on the sky. Given the required high luminosity for the exciting source and accurate positions for the center of expansion in many H_2O maser sources, it is surprising that observations both at infrared and radio wavelengths often fail to detect evidence of the central star.

The reasons for the difficulty in detecting a central star in powerful interstellar H_2O masers can be traced to a combination of circumstances. Primarily, regions of massive star formation are often crowded with luminous objects and are usually at large distances ($\gtrsim 1$ kpc). Commonly, H_2O masers are found near, but not directly associated with, ultracompact H II (UCH II) regions. UCH II regions emit intense free-free radiation, often ~ 1 Jy at centimeter wavelengths. At these wavelengths, only interferometers (such as the VLA) can achieve (sub)arcsecond imaging, but most radio images of these complex regions have been limited in dynamic range to detections of relatively strong sources ($\gtrsim 10$ mJy).

Dust associated with UCH II regions is strongly heated and radiates copiously in the infrared. In order to detect (potentially) weak and deeply embedded sources in such fields, imaging systems must have an angular resolution approaching 1″ and very high dynamic range. Observations at wavelengths longer than a few microns are needed to detect deeply imbedded sources and, until recently, few systems have achieved the required sensitivity and resolution to attempt such observations.

Given the paucity of observations that might elucidate the nature of the exciting sources of powerful H_2O masers, only a sketchy and speculative picture has been suggested which has the following elements. At the center of a H_2O maser complex is a recently formed OB-type star (or stars). Water masers are dense cloudlets accelerated to high velocities (sometimes hundreds of km s^{-1}), possibly by tapping into magnetic or rotational energy or the powerful winds of the star. Although an O- or early B-type star has copious ionizing photons, the plasma surrounding the star is so dense that a balance of ionization and rapid recombination results in a "supercompact" H II region. This H II region, because of its extremely small size, may be a very weak, or undetectable, radio continuum source.

In this paper, we show evidence that, instead of finding weak thermal emission from a "supercompact" H II region, we have detected what appears to be *nonthermal* radio continuum emission toward the center of the H_2O maser outflow and near the dense, compact molecular clump detected in HCN emission by Turner & Welch (1984) near the UCH II region W3(OH). Perhaps the simplest explanation for nonthermal emission is that some electrons are accelerated to relativistic speeds by a Fermi process in a region of strong shocks and radiate by the synchrotron emission process. Thus, the unanticipated finding of synchrotron emission associated with an interstellar H_2O maser provides direct evidence for the presence of shocks, previously suggested on theoretical grounds (e.g., Hollenbach & McKee 1989; Neufeld & Dalgarno 1989).

2. OBSERVATIONS AND RESULTS

The W3(OH) region, shown in Figure 1, contains at least two sites where massive stars have formed within a projected distance of 0.1 pc. The most prominent site, based upon infrared and radio frequency emissions, is the UCH II region near R.A. = $02^h23^m16^s.50$ and decl. = 61°38′57″.2 (B1950). This UCH II region is a 3 Jy continuum source, above its turnover frequency of ≈ 12 GHz, and is the location of strong OH and CH_3OH masers (Menten et al. 1992). Approximately 6″ to the

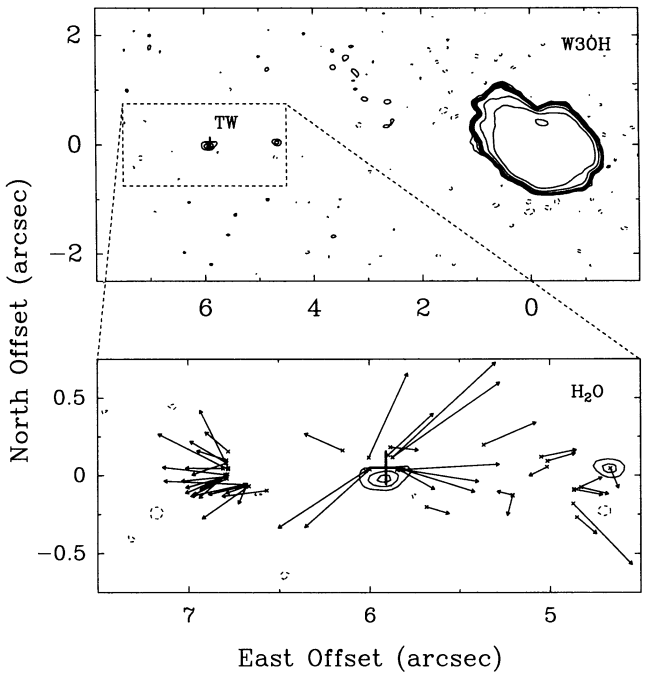

FIG. 1.—*Upper panel*: Continuum emission from the W3(OH) region at 15 GHz. Contours are at −0.15, 0.15, 0.30, 0.45, 0.60, 0.75, 1, 3, 10, and 30 mJy beam^{-1}. The most intense emission is from the ultracompact H II region at the origin of the map. Approximately 6″ eastward is the position of the Turner-Welch object (Turner & Welch 1984), labeled TW, and the center of the H_2O masers (indicated by the cross), from Alcolea et al. (1992). Weak continuum emission, the topic of this paper, is detected at (5″.92, −0″.01), corresponding to R.A. = 02^{h}23^{m}17^s.330 and decl. = 61°38′57″.20 (B1950). *Lower panel*: Expanded view of the continuum emission near the TW object. The positions and proper motions of the H_2O masers are indicated by arrows. The continuum source at (5″.92, −0″.01) lies within 0″.1 (3×10^{15} cm) of the center of expansion of the H_2O masers.

east of the UCH II region is a complex of strong H_2O masers. Turner & Welch (1984) detected compact HCN emission from a dense, warm clump of molecular gas close to the H_2O masers, indicating a luminous object near that position. This was the first published detection of this interesting source and we will refer to it as the Turner-Welch (TW) object. Subsequently, Wink et al. (1994) reported detections of other molecular species toward the TW object. Note the detection, in Figure 1, of weak continuum emission offset from the origin of the map by 5″.92 and −0″.01 toward the east and north, respectively. Combining results from our 15 and 8 GHz maps we determined the position of this continuum source to be R.A. = 02^{h}23^{m}17^s.330 and decl. = 61°38′57″.20 (B1950), with an uncertainty of about 0″.05. Note that the continuum source is almost precisely (within 0″.1 or 3×10^{15} cm) at the position of the center of expansion of the H_2O masers (Alcolea et al. 1992), and near the position of the TW object.

In Figure 2 we plot the flux density and angular size of the continuum source near the position of the H_2O masers and TW object. The six observations used to define this spectrum include those reported by Guilloteau et al. (1985) and Baudry et al. (1993) and are listed in Table 1. Five were obtained with the NRAO[1] VLA in its largest (A) configuration and one in a smaller (B) configuration. (Weighted averages of the flux density and angular size for the three 8 GHz observations are displayed in Fig. 2.) The spectrum of the continuum source between 1.6 and 15 GHz exhibits a flux density, S_ν, decreasing with frequency, ν, as a power law with $S_\nu \propto \nu^{-0.6\pm0.1}$. The source is elongated approximately in the east–west direction and its intrinsic size in this direction, θ_{maj}, defined as the full-width at half-maximum (FWHM) for the major axis of an elliptical Gaussian model, decreases with frequency as $\theta_{maj} \propto \nu^{-1.0\pm0.2}$. The source appears either marginally resolved or unresolved in the north–south direction at all frequencies, providing an upper limit of about two-thirds of the east–west size. This implies a brightness temperature greater than $500 \times (\nu/10\ \mathrm{GHz})^{-0.6}$ K. We also find some continuum emission near the western boundary of the H_2O masers in the 15 GHz map (Fig. 1) and in the A-configuration maps at 8 GHz. Unfortunately, this emission is too weak to obtain significant limits on the spectral index and size with current data.

[1] NRAO is operated by Associated Universities, Inc., in a cooperative agreement with the National Science Foundation.

TABLE 1

RADIO CONTINUUM EMISSION NEAR THE H_2O MASERS/TW OBJECT IN W3(OH)[a]

Observing Frequency (GHz)	VLA Configuration	Beam Size	Flux Density (mJy)	Major Axis[b]	Reference
1.6	A	0″.9	2.5 ± 0.7	1″.4 ± 0″.4	This paper[c]
4.7	A	0.5	1.5 ± 0.3	s.e.[d]	Guilloteau et al. 1985
8.2	A	0.3	1.2 ± 0.5	s.e.[d]	Baudry et al. 1993
8.3	A	0.3	0.9 ± 0.2	0.34 ± 0.1	Keto et al. 1994[e]
8.4	B	1.1[f]	1.1 ± 0.2	0.37 ± 0.3	This paper[f]
14.7	A	0.2	0.75 ± 0.15	0.16 ± 0.05	This paper[g]

[a] Position of the continuum emission is R.A. = 02^{h}23^{m}17^s.330 and decl. = 61°38′57″.20 (B1950).

[b] Intrinsic (or deconvolved) source size. The major axis was near 90° position angle, and the minor axis size was less than two-thirds of the major axis size.

[c] Observations on 1993 November 12 spanning 3 hr centered at 01^{h}00^m LST and using a 12.5 MHz band in RCP and LCP.

[d] Described as "slightly extended" (s.e.) or resolved in the original reference.

[e] Observations on 1988 November 3 spanning 8 hr centered at 04^{h}10^m LST and using an effective bandwidth of 4.7 MHz in RCP and LCP.

[f] Geometric mean of the 2″.5 by 0″.5 beam at position angle −40° afforded by a 1 hr observation near 17^{h}30^m LST on 1991 November 9.

[g] Observations on 1986 March 6 spanning 8.5 hr and using a 50 MHz bandwidth in RCP and LCP.

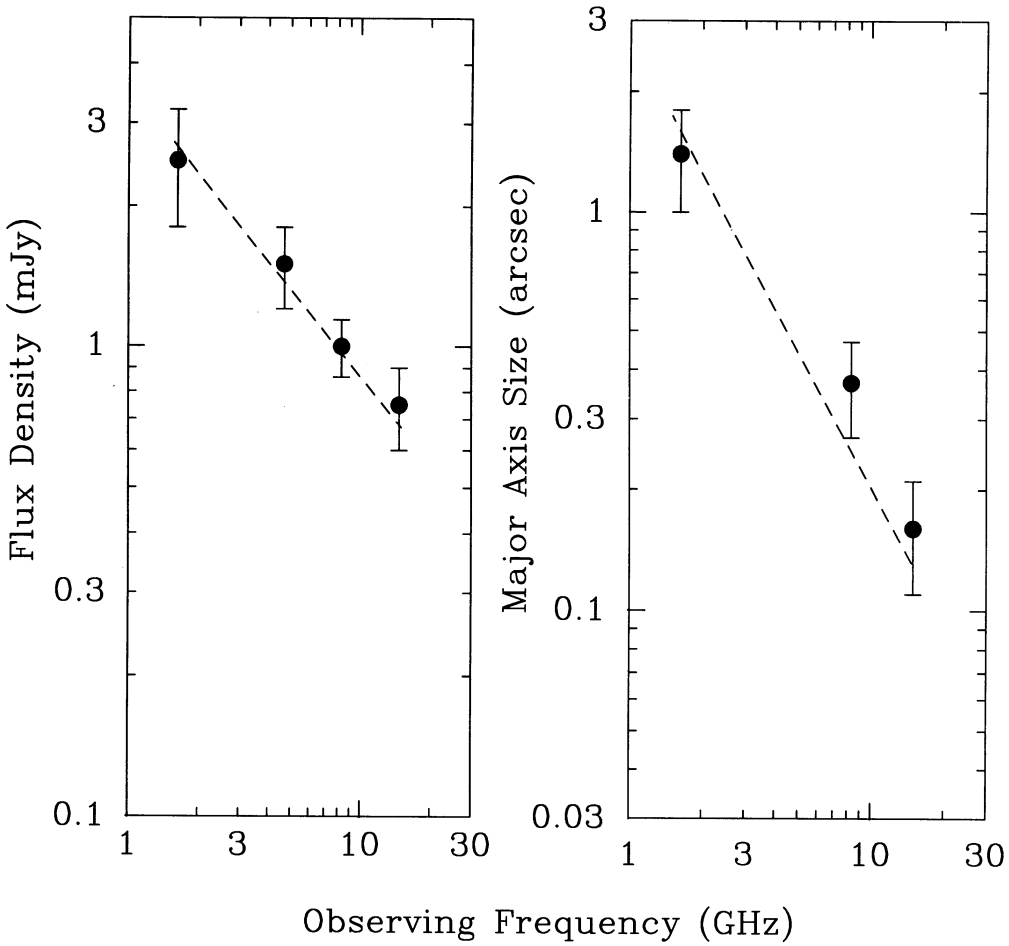

FIG. 2.—Continuum emission near the TW/H_2O source in W3(OH). *Left panel*: Total flux density vs. observing frequency measured from VLA maps; the dashed line corresponds to that expected for the synchrotron source model described in the text. *Right panel*: Angular size (FWHM) in the east–west direction vs. observing frequency; the dashed line corresponds to the size expected for the synchrotron source model.

3. DISCUSSION

3.1. *Emission Mechanism: Thermal or Synchrotron?*

The spectrum of the continuum source near the position of the H_2O masers and TW object in the W3(OH) region, shown in Figure 2, appears inconsistent with that expected for thermal emission. Rodríguez et al. (1993) show that sharply negative spectral indices cannot occur for thermal processes involving free-free emission and absorption, regardless of the electron density and temperature distribution. They conclude that a thermal bremsstrahlung source could display a sharply negative spectral index only if the intrinsic source is optically thin (with spectral index of -0.1) and significant dust absorption extends to the lowest frequencies observed. For W3(OH) this would require extraordinary amounts of dust, since greater than centimeter-size "grains" are needed to absorb 1 GHz photons efficiently. Thus, thermal emission, even with a component of absorption by dust, does not seem to be a viable model for this source.

Most of the data reported in this paper came from the VLA in its largest (A) configuration, where the synthesized beam size decrease linearly with increasing frequency. This raises the question of whether the source size variation is related to the synthesized beam size or the observing wavelength. An optically thin source whose volume emissivity, j_ν, follows a power law in radius, r (i.e., $j_\nu \propto r^{-\alpha}$), has no intrinsic size and its *apparent* size would follow the observing beam, θ_b. For example, a spherical source with $j_\nu \propto r^{-2}$, where r is the distance from the center of the source, would display an apparent source size, defined as the FWHM, of $\approx 1.6\theta_b$, approximately as observed for the A configuration data. Such a source could exhibit an *apparent* spectrum considerably steeper than expected for a uniform source, since lower frequency observations made with a larger beam would integrate over more of the source and register a greater flux density than at higher frequencies. However, it can be demonstrated that this is not the case for the TW/H_2O maser source in W3(OH), since we have maps with two different resolutions near one frequency (8 GHz). While the smaller (B) configuration observations at 8 GHz have a synthesized beam area ~ 10 times greater than for the larger (A) configuration observations, the source flux density and size are nearly the same in the A and B configuration maps. Thus the continuum emission from the TW/H_2O source has a size that is predominantly wavelength-dependent and not due to instrumental limitations.

The spectral and source size characteristics can be explained by a model of incoherent synchrotron emission. The observed spectral index is typical of optically thin synchrotron sources,

such as from active galactic nuclei, contact binaries (e.g., SS 433), and supernova remnants. The elongated source shape, with (major-axis) size decreasing with increasing frequency, is a common feature of active galactic nuclei (and the Galactic source SS 433) where jetlike emissions are observed. However, it is not common to have synchrotron emission from jets in active galactic nuclei with the combination of a negative spectral index *and* an apparent source size decreasing with frequency as observed in W3(OH).

Spectral indices of radio sources are bounded by their optically thick and thin limits. For synchrotron emission these limits are $S \propto \nu^{2.5}$ for optically thick and $S \propto \nu^{-(p-1)/2}$ for optically thin emission, where p is the electron energy index defined below in equation (1). The essential problem in explaining the apparent size variation with frequency, shown in Figure 2, is that the source must have significant opacity ($\tau \gtrsim 1$) over the range of observed frequencies. High opacity, however, will tend to drive the spectral index toward the optically thick limit of +2.5, which is not observed. The solution to this dilemma requires a source whose physical properties change with radius, allowing the "$\tau = 1$" surface to decrease in size rapidly with observing frequency.

3.2. *Synchrotron Model*

3.2.1. *Model Definition*

Following the analysis of de Bruyn (1976), we have constructed a simple model of a nonuniform synchrotron source with significant self-absorption that can fit the data surprisingly well. The model, designed to approximate a jetlike source, consists of a biconical-like structure elongated in the east–west direction on the plane of the sky. The opening angle of the "cones" was set arbitrarily at 0.1 radians and, in order to simplify the radiative transfer calculations, the cross section of a "cone" was made square instead of circular. Thus, the depth (along the line of sight) and width (in the north–south direction) of a "cone" at any radius, r, is given by $z(r) = 0.1r$. The model allows for a decrease in the (relativistic) electron density, $N_{re}(\gamma, r)$, and magnetic field strength, $B(r)$, via power laws in radius as follows:

$$N_{re}(\gamma, r) = N_0 \gamma^{-p} \left(\frac{r}{r_0}\right)^{-n} \quad (1)$$

and

$$B(r) = B_0 \left(\frac{r}{r_0}\right)^{-m} , \quad (2)$$

where γ is the ratio of the electron kinetic energy to its rest-mass energy. Adjustable parameters are the values, at a radial distance r_0, of the electron density, N_0, and the magnetic field, B_0, and the exponents of the power laws for the electron energy, p, the electron density, n, and the magnetic field, m. The intensity as a function of radius, $I_\nu(r)$, is given by

$$I_\nu(r) = \frac{j_\nu(r)}{\alpha_\nu(r)} [1 - e^{-\alpha_\nu(r) z(r)}] , \quad (3)$$

where j_ν and α_ν are the emission and absorption coefficients, respectively, for synchrotron processes which depend on $N_{re}(\gamma, r)$ and $B(r)$ (see, e.g., Rybicki & Lightman 1979). The flux density as a function of radius, $S_\nu\, dr$, can then be obtained from equation (3):

$$S_\nu(r)dr = \frac{1}{D^2} I_\nu(r) z(r) dr , \quad (4)$$

where D is the distance to W3(OH). A theoretical value for the total flux density can be obtained by integrating equation (4) over all radii. In practice, the source cannot extend from $r = 0$ to ∞, and for power laws the flux density integral can diverge. Thus, we assume inner and outer radial limits of 3.3×10^{13} (0".001) and 6.6×10^{16} cm (2"); varying these limits does not significantly affect the model for the ranges of parameters discussed in this paper.

Before proceeding with a numerical evaluation of the model and fitting of the data, we present a crude, but instructive, approximation that allows a simple characterization of the synchrotron model. We approximate the source size as that given by the unity optical depth (τ_ν) surface, where $\tau_\nu = \int \alpha_\nu dz \propto \alpha_\nu r$. Since $\alpha_\nu \propto N_{re} B^{(p+2)/2} \nu^{-(p+4)/2}$ and only considering parameters that vary with radius or frequency, we find

$$\tau_\nu \propto N_{re} B^{(p+2)/2} \nu^{-(p+4)/2} r . \quad (5)$$

For N_{re} and B given by the radial power laws of equations (1) and (2), setting $\tau_\nu = 1$ in equation (5) requires

$$r \propto \nu^{(p+4)/[2-2n-m(p+2)]} . \quad (6)$$

The flux density of the source, S_ν, can be approximated as the product of the synchrotron source function, j_ν/α_ν, and the source solid angle. Since $j_\nu \propto N_{re} B^{(p+1)/2} \nu^{-(p-1)/2}$ and the solid angle is proportional to r^2, we obtain

$$S_\nu \propto r^{(4+m)/2} \nu^{5/2} . \quad (7)$$

Inserting r from equation (6) into equation (7) leads to

$$S_\nu \propto \nu^{\{(p+4)/[2-2n-m(p+2)]\}[(m+4)/2]+5/2} . \quad (8)$$

For the parameters derived below by numerically evaluating the model and fitting to the data ($p = 2$, $n = 1.6$, and $m = 0.8$), equations (6) and (8) imply $r \propto \nu^{-1.4}$ and $S_\nu \propto \nu^{-0.8}$, respectively. These dependencies are comparable to those observed for the TW/H_2O source.

3.2.2. *Numerical Evaluation and Model Fit Results*

The crude analysis based upon a "$\tau = 1$" surface approximation was followed by a detailed numerical modeling procedure. We numerically evaluated equation (4) over a grid of 1000 points equally spaced in r between the inner and outer limits. A *theoretical* flux density was obtained by summing the flux density from each grid point. However, the source size is not easily defined since the model described by equation (4) rises from $S_\nu = 0$ at $r = 0$ to a peak near the radius at which $\tau = 1$, before falling back toward zero as the source becomes thin and j_ν decreases with increasing radius. For a symmetric, two-sided, emission pattern (which peaks at two positions on the sky), the definition of a single source-size parameter is somewhat arbitrary. We chose to follow a definition that matched our observational procedure for estimating source size (and total flux density). At each observing frequency, we calculated a model flux density profile from equation (4), convolved this profile with an instrumental beam appropriate for the VLA A configuration, and fitted a Gaussian profile by

matching it to the peak and FWHM of the convolved-model profile.

Our procedure to adjust model parameters to best fit the data treated the four flux density and the three size measurements shown in Figure 2 as observed data. Model values of flux density and size were numerically evaluated as described above, along with the partial derivatives of the model with respect to each adjustable parameter. We then iteratively adjusted the parameters to minimize the weighted sum of the squares of the deviation of the model from the observed data. We were able to fit the data well with the following parameter values: $N_0 = 0.068$ cm^{-3} and $B_0 = 0.01$ G, at $r_0 = 0\farcs2$ (i.e., 6.6×10^{15} cm at a distance of 2.2 kpc), and $p = 2.0$, $n = 1.6$, and $m = 0.8$.

We found high correlations among some of the parameters, and we were not able to solve for all parameters simultaneously. For example, N_0 and B_0 were very highly correlated, probably because (for $p = 2$) $j_\nu \propto N_0 B_0^{3/2}$ and the source size at $\tau = 1$ is proportional to $(N_0 B_0^2)^{-1}$. Indeed, we found that an increase (or decrease) of B_0 by a factor of 10 required a corresponding decrease (or increase) of N_0 by a factor of about 30. Changing B_0 by more than about an order of magnitude noticeably degraded the fits. The adopted value of $B_0 = 0.01$ G is close to that which minimizes the total energy in particles and fields and also close to measured magnetic field strengths in H_2O sources (Fiebig & Güsten 1989). In order to limit the number of free parameters, we set $m = n/2$. This requires $B \propto N_{\rm re}^{1/2}$; some justification for this relation can be found in magnetic field measurements of dense molecular material where $B \propto N_{\rm H_2}^{1/2}$ is observed over a wide range of densities in star-forming regions (e.g., Fiebig & Güsten 1989). Removing this restriction, we found a slightly improved fit to the data with constant density ($n = 0$) and magnetic field strength falling as r^{-2} (i.e., $m = 2$). Essentially, values of n and m that satisfy the relation $m = 2 - 0.73n$ produce a reasonable match to the data. This relation between n and m results approximately in $j_\nu \propto r^{-3}$.

The most robust parameter in the model is the electron energy index, p. All fits to the data arrived at $p = 2.00$ within a 3% formal uncertainty. Forcing p to values of 2.05 and 1.90 produced significantly poorer fits to the data. It is interesting to note that $N_{\rm re}(\gamma) \propto \gamma^{-2}$ is the theoretically predicted value for electron acceleration via a first-order Fermi process involving strong shocks (e.g., Bell 1978). Most likely, p is strongly constrained by the spectral information. For the model presented above, a one-dimensional flux density profile starting at the center of the source rises rapidly to a peak, which occurs near $\tau = 1$, and then falls more gradually as the source becomes optically thin. This behavior is shown in the left-hand panel of Figure 3. The majority of the emission comes from the outer (optically thin) portion of the source and in this regime the flux density and electron energy index are directly related by $S \propto \nu^{-(p-1)/2}$.

Given a value for p, we can calculate the total density of relativistic electrons, $N_{\rm re}$, by integrating from low to high electron energy limits, γ_l to γ_h, respectively,

$$N_{\rm re} = \int_{\gamma_l}^{\gamma_h} N_0 \gamma^{-p} d\gamma \, . \tag{9}$$

For $p = 2$, most of the electrons are at the lowest energies, and equation (9) yields

$$N_{\rm re} \approx \frac{N_0}{\gamma_l} \, . \tag{10}$$

For a low-energy limit of $\gamma_l = 15$, corresponding to a low-frequency limit of about 10 MHz, the total density of *relativistic* electrons is about 5×10^{-3} cm^{-3} (at $r = r_0 = 0\farcs2$).

3.2.3. *Observation and Model Bias*

One aspect of our fitting process needs further discussion. We achieve a good fit to the flux density and size data with an electron index of $p = 2$, which yields an optically thin spectral index of -0.5. Yet, the model spectrum shown in Figure 2 has a spectral index of -0.6, somewhat steeper than theoretically allowed. This occurs because our modeling analysis mimics our observational approach for estimating source parameters. As mentioned above, at each observing frequency, we calculate a model flux density profile using equation (4), convolve this profile with an instrumental beam appropriate for the VLA A configuration data, and fit a Gaussian profile by matching it to the peak and FWHM of the convolved-model profile. Were the model profiles Gaussian in shape, the fitting procedure would be rigorously correct. However, the model profiles display long tails and are distinctly non-Gaussian.

Figure 3 displays flux-density profiles for our lowest and highest observing frequencies for the pure model, for the model convolved with the VLA beam, and the Gaussian fits to the convolved profiles. The Gaussian fits increasingly underestimate the total (integrated) flux density as one goes to higher observing frequency. This causes the *apparent* spectrum, generated from Gaussian fits, to be steeper than for the pure model. For the best-fitting parameters given above, the *theoretical* spectral index, derived by directly evaluating equation (4), is about -0.3, which is flatter than the optically thin value of -0.5 appropriate for an energy index of $p = 2$. Clearly extreme caution is appropriate when obtaining spectral indices from radio maps, even when beam sizes are matched at different observing frequencies. Unfortunately, the source in W3(OH) is weak and difficult to map. Given the present observations it is not possible to detect convincingly non-Gaussian source profiles at the levels suggested by the convolved-model profiles.

3.3. *Limits on a Thermal Component*

We tried to fit a pure thermal model to the observed flux density and size data, but could not find an acceptable fit. The thermal bremsstrahlung model used the same geometry as the synchrotron model and allowed for a power-law decrease in thermal density and a power-law decrease in temperature with radius. The best-fit thermal model resulted in a slightly rising spectrum ($S \propto \nu^{0.2}$) and sizes approximately a factor of 2 larger than observed. We could force a thermal model to yield a good match to the source spectrum, but, for electron temperatures below 10^5 K, this required source sizes significantly greater than observed. Also, for the models examined, the non-Gaussian tails of the flux density profiles were large enough that they would have been detected with either the A or B configuration VLA data at 8 GHz. We conclude that a pure thermal model cannot fit our data.

While a pure synchrotron-emitting source can (and a pure thermal source cannot) fit the observational data, it is likely that some thermal plasma is mixed in with or surrounding the relativistic electrons. The addition of a small component of thermal emission to the synchrotron emission would be most noticeable at our highest frequency of 15 GHz, since thermal emission has a flat or rising spectrum. The source spectrum, shown in Figure 2, is well-characterized by a single power law. Unless one considers the unlikely combination of a simultaneous steepening of the synchrotron spectrum and a counter-

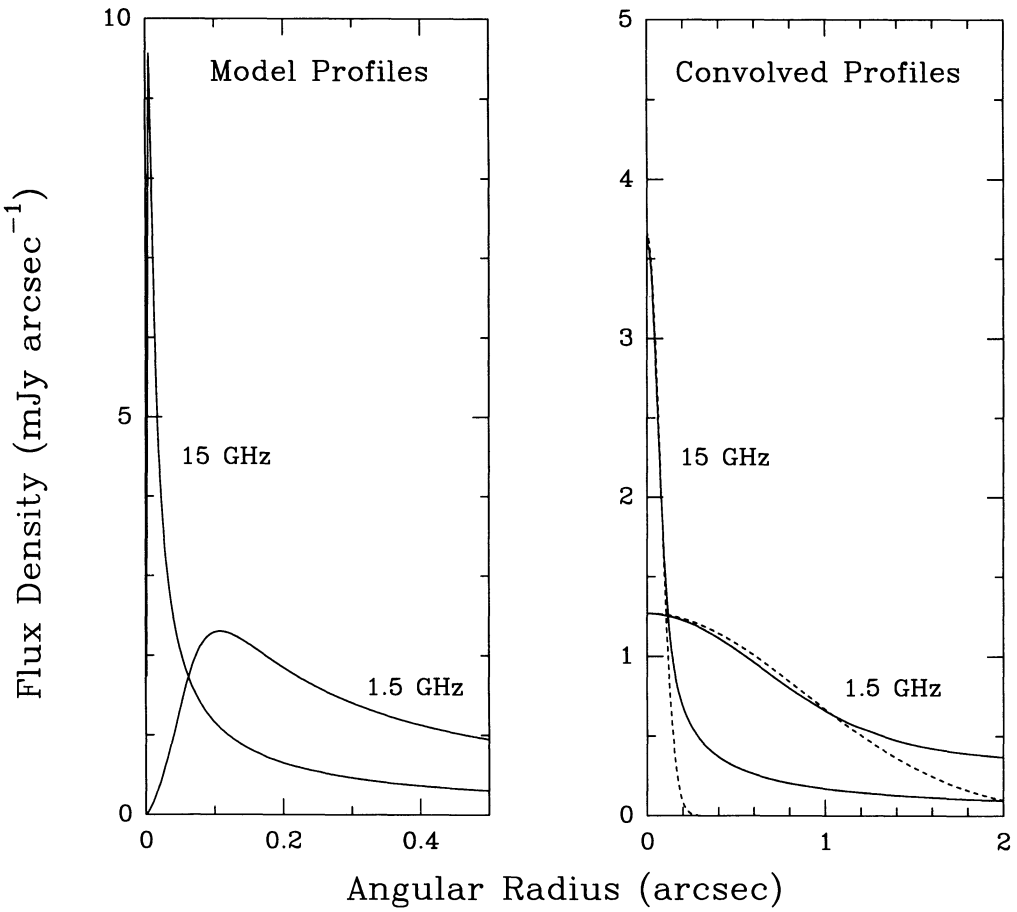

FIG. 3.—Flux density profiles at 1.5 and 15 GHz. *Left panel*: The inner 0".5 radial profile of the synchrotron model described in the text, and *Right panel*: the full 2" profiles convolved with the synthesized interferometer beam (*solid lines*) appropriate for the A configuration of the VLA, and Gaussian fits to the convolved profiles (*dashed lines*).

balancing addition of a rising thermal component, the data could be interpreted to require that less than about 0.2 mJy of the 15 GHz flux density comes from thermal emission. It is difficult to be more specific regarding an upper limit on a thermal component, without specifying the radial distribution of thermal electrons. However, we investigated a variety of distributions of thermal electron density and conclude that densities exceeding about 2×10^5 cm^{-3} (at $r = 0''.2$) would have contributed noticeably at 15 GHz and degraded the model fits. This provides some indications of an upper limit to the thermal plasma mixed in the synchrotron-emitting region.

3.4. *Future Observation*

The model presented above makes predictions that can be tested with future observations. A direct verification of the presence of synchrotron emission would be the detection of a significant component of linear polarization. Given current capabilities for the VLA at a frequency of 8 GHz, one could expect to detect linear polarization at about 10% of the total intensity with observations of less than 1 day duration. Unfortunately, should linearly polarized emission not be detected, one could not rule out synchrotron emission, since the observation of net polarization requires ordered magnetic fields and negligible Faraday rotation in the thermal plasma. Another test of the model presented above would involve searching for the non-Gaussian tails predicted for the flux-density profiles. This could also be attempted with more sensitive VLA observations than presented in this paper. Finally, observations with higher angular resolution are needed in order to determine how narrow the emission is in the north–south direction. This will require longer baselines than available with the VLA; possibly the MERLIN array or the inner antennas of the Very Long Baseline Array, in conjunction with the VLA, can be used to achieve the necessary sensitivity and angular resolution.

4. SPECULATIONS

H_2O masers often exhibit energetic outflows, with observed outflow speeds of up to a few hundred km s^{-1} and mass loss rates of up to $10^{-3}\ M_\odot$ yr^{-1}. These characteristics require a very luminous central source and have led to the hypothesis that a forming or recently formed O-type star is involved. Since nonthermal emission has been detected toward O-type stars, such as Cyg OB2 and 9 Sgr, with fast (1000–3000 km s^{-1}) winds (e.g., White 1985; Bieging, Abbott, & Churchwell 1989), the detection of nonthermal emission from the H_2O masers in W3(OH) adds weight to the hypothesis that interstellar H_2O masers are powered by O-type stars.

Extreme O-type stars, such as Cyg OB2 and 9 Sgr, with nonthermal emissions have spectral types earlier than O5, masses of $\sim 100\ M_\odot$, and luminosities of $\sim 10^6\ L_\odot$. These stars are at distances of $\gtrsim 2$ kpc, have observed flux densities of ~ 1

mJy at centimeter wavelengths, and have negative spectral indexes. Thus, many features of very luminous H_2O maser sources, such as in W49 and Sgr B2, could be explained with embedded stars like Cyg OB2 and 9 Sgr. While extreme O-type stars may power the strongest interstellar H_2O maser sources, they are too luminous to be consistent with observations of the W3(OH) source. The W3(OH) H_2O masers are about 2 or 3 orders of magnitude less luminous than Sgr B2 or W49, respectively, assuming similar maser-beaming angles. Similarly, most of the $\sim 10^5\ L_\odot$ coming from the W3(OH) region as infrared emission originates from the UCH II region (Campbell et al. 1989), approximately 6″ west of the center of expansion of the H_2O masers. Thus, the central star powering the H_2O masers in W3(OH) must have a luminosity considerably less than $\sim 10^5\ L_\odot$; a late O-type or early B-type star is a possible candidate.

Proper motions of the H_2O masers in W3(OH) by Alcolea et al. (1993) indicate a bipolar outflow. As shown in Figure 1, the center of the outflow is within 0.″1 of the peak of the nonthermal continuum emission. The H_2O outflow speed is about 20 km s^{-1}, and the distribution and motions of the maser spots are predominantly in the east–west direction. Thus the H_2O outflow has the same position and is elongated in nearly the same direction as the nonthermal continuum emission, suggesting a causal connection.

A qualitative model that can account for the observations of W3(OH) might involve a late O-type or early B-type star, with a fast stellar wind. This wind is collimated and drives a jet in the east–west direction. Fast shocks in the wind or associated jet accelerate electrons to relativistic speeds via a Fermi mechanism (see Chen & White 1993). It is likely that at some distance from the central source the ram pressure of the wind will be balanced by magnetic pressures in the postshocked gas. In this case an appropriate model might involve the wind density decreasing as r^{-2} (i.e., $n = 2$) and, therefore, the magnetic field decreasing as r^{-1} (i.e., $m = 1$). These conditions are similar to those in presented § 3.2.2 and consistent with the data. As the collimated wind or jet impinges on the surrounding molecular material, it further shocks and accelerates this material. The postshocked regions will be dense and have high temperatures and water is formed efficiently. The H_2O masers may be pumped collisionally, as proposed for J-type shocks by Elitzur, Hollenbach, & McKee (1989) or for C-type shocks by Melnick et al. (1993), or pumped by infrared radiation (e.g., Tarter & Welch 1986).

We wish to thank Mercè Crosas, Guido Garay, and Lincoln Greenhill for interesting discussions regarding this paper, and John Kawamura for helping to make the 15 GHz map.

REFERENCES

Alcolea, J., Menten, K. M., Moran, J. M., & Reid, M. J. 1992, in Astrophysical Masers, ed. A. W. Clegg & G. E. Nedoluha (Heidelberg: Springer), 225
Baudry, A., Menten, K. M., Walmsley, C. M., & Wilson, T. L. 1993, A&A, 271, 552
Bell, A. R. 1978, MNRAS, 182, 147
Bieging, J. H., Abbott, D. C., & Churchwell, E. B. 1989, ApJ, 340, 518
Campbell, M. F., Lester, D. F., Harvey, P. M., & Joy, M. 1989, ApJ, 345, 298
Chen, W., & White, R. L. 1993, ApJ, 366, 512
de Bruyn, A. G. 1976, A&A, 52, 439
Elitzur, M., Hollenbach, D. J., & McKee, C. F. 1989, ApJ, 346, 983
Fiebig, D., & Güsten, R. 1989, A&A, 214, 333
Genzel, R., Reid, M. J., Moran, J. M., & Downes, D. 1981, ApJ, 244, 884
Guilloteau, S., Brudry, A., & Walmsley, C. M. 1985, A&A, 153, 179
Gwinn, C. R., Moran, J. M., & Reid, M. J. 1992, ApJ, 393, 149
Hollenbach, D. J., & McKee, C. F. 1989, ApJ, 342, 306
Keto, E. R., Welch, W. J., Reid, M. J., & Ho, P. T. P. 1994, ApJ, submitted
Melnick, G., Menten, K. M., Phillips, T. G., & Hunter, T. 1993, ApJ, 416, L37
Menten, K. M., Reid, M. J., Pratap, P., Moran, J. M., & Wilson, T. L. 1992, ApJ, 401, L39
Neufeld, D. A., & Dalgarno, A. 1989, ApJ, 340, 869
Reid, M. J., Schneps, M. H., Moran, J. M., Gwinn, C. R., Genzel, R., Downes, D., & Rönnäng 1988, ApJ, 330, 809
Rodríguez, L. F., Martí, J., Cantó, J., Moran, J. M., & Curiel, S. 1993, Rev. Mexicana Astron. Af., 25, 23
Rybicki, G. B., & Lightman, A. P. 1979, Radiative Processes in Astrophysics (New York: Wiley)
Tarter, J. C., & Welch, W. J. 1986, ApJ, 305, 467
Turner, J. L., & Welch, W. J. 1984, ApJ, 287, L81
White, R. L. 1985, ApJ, 289, 698
Wink, J. E., Duvert, G., Guilloteau, S., Güsten, R., Walmsley, C. M., & Wilson, T. L. 1994, A&A, 281, 505